

# Low temperature metallic state induced by electrostatic carrier doping of SrTiO<sub>3</sub>

H. Nakamura,<sup>1,2</sup> I. H. Inoue,<sup>1</sup> H. Takagi,<sup>1,2</sup> Y. Takahashi,<sup>1</sup> T. Hasegawa,<sup>1</sup> and Y. Tokura<sup>1,3</sup>

<sup>1</sup>*Correlated Electron Research Center (CERC),  
National Institute of Advanced Industrial Science and Technology (AIST),  
Tsukuba 305-8562, Japan*

<sup>2</sup>*Department of Advanced Materials, University of Tokyo, Kashiwa 277-8581, Japan.*

<sup>3</sup>*Department of Applied Physics, University of Tokyo, Tokyo 113-8656, Japan*

(Dated: July 11, 2018)

Transport properties of SrTiO<sub>3</sub>-channel field-effect transistors with parylene organic gate insulator have been investigated. By applying gate voltage, the sheet resistance falls below  $R_{\square} \sim 10 \text{ k}\Omega$  at low temperatures, with carrier mobility exceeding  $1000 \text{ cm}^2/\text{Vs}$ . The temperature dependence of the sheet resistance taken under constant gate voltage exhibits metallic behavior ( $dR/dT > 0$ ). Our results demonstrate an insulator to metal transition in SrTiO<sub>3</sub> driven by electrostatic carrier density control.

Electronic properties of transition-metal oxides, including high-temperature superconductivity in cuprates and colossal magnetoresistance in manganites, are currently an area of active research [1]. These exotic phases are crucially dependent on the density of carriers in the system; for example, superconductivity in cuprates appears only at a certain range of carrier concentration. Electrostatic carrier doping is an attractive approach in this research field, because unlike chemical doping of carriers—a conventional method introducing lattice disorder—it enables us to tune only the carrier concentration of materials under investigation [2, 3]. Among transition-metal oxides, here we focus on SrTiO<sub>3</sub>, a wide-gap insulator ( $E_g = 3.2 \text{ eV}$ ) with a cubic-perovskite structure. By chemical doping, SrTiO<sub>3</sub> becomes metallic, and by further doping becomes a superconductor. Interestingly, these transitions are reported to occur at low carrier concentrations of  $10^{18} \text{ cm}^{-3}$  and  $10^{19} \text{ cm}^{-3}$ , respectively [4, 5]. Since they are within a range accessible by electrostatic carrier doping, the two phases may be observed by electrostatic carrier doping of an undoped, insulating sample.

Recent attempts [6, 7] to use undoped SrTiO<sub>3</sub> as the active channel of a field-effect transistor (FET) have faced a common problem: carrier injection from the source/drain electrodes becomes increasingly difficult with decreasing temperature. Even with a large applied gate electric field, the channel resistance increases monotonically as temperature decreases [6]. The origin may be trap levels in the SrTiO<sub>3</sub> channel, and/or barrier formation at the interface between the metal electrodes and the SrTiO<sub>3</sub> channel.

In this work, we attempted to realize a low temperature metallic state in SrTiO<sub>3</sub>-FET by solving this problem. Our strategy is as follows: First, we improve the quality of electrodes to improve the metal-electrode/SrTiO<sub>3</sub>-channel interface. Next, we adopt an organic polymer, parylene, for a gate insulator to minimize traps at the gate-insulator/SrTiO<sub>3</sub>-channel interface. Finally, we introduce two potential probes just inside the channel region to perform a four-probe measurement to determine the intrinsic channel properties. In

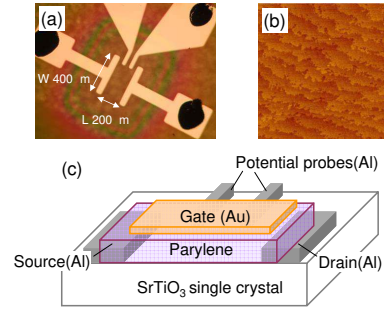


FIG. 1: (a) Photograph of our SrTiO<sub>3</sub>-FET device taken just after the deposition of the parylene gate insulator. (b) An image of the pristine SrTiO<sub>3</sub> (100) surface taken by atomic force microscopy before device fabrication. Displayed area is  $2 \mu\text{m} \times 2 \mu\text{m}$ . (c) Schematic structure of SrTiO<sub>3</sub>-FET. Thickness of the aluminum electrodes is 20 nm and that of gate electrode is 40 nm.

this paper, we describe successful carrier injection at low temperatures using these strategies, and demonstrate an electric-field-induced insulator-to-metal transition on an undoped SrTiO<sub>3</sub> single crystal.

The device structure is shown in Fig. 1, which was formed on the (100) surface of undoped SrTiO<sub>3</sub> single crystals. (The crystals had been polished and etched by a vendor following Ref. 8.) The 20 nm thick aluminum electrodes were evaporated by resistive heating using a tungsten boat under a pressure of  $10^{-4} \text{ Pa}$ . Next, the parylene insulator ( $\epsilon_r = 3.15$ ) was deposited by first pyrolyzing the monomer at  $700^\circ\text{C}$ , and the polymerization on the SrTiO<sub>3</sub> substrate held at room temperature. It should be noted that the deposition conditions, for aluminum and parylene, markedly affects the device performance at low temperatures, although many of the devices show almost identical characteristics at room temperature. We found that the key issue is the degree of vacuum during the deposition of parylene. The base pressure in which we deposit the parylene must be kept lower than  $3 \times 10^{-4} \text{ Pa}$  to prevent the oxidization of aluminum, although the deposition of the parylene itself does not

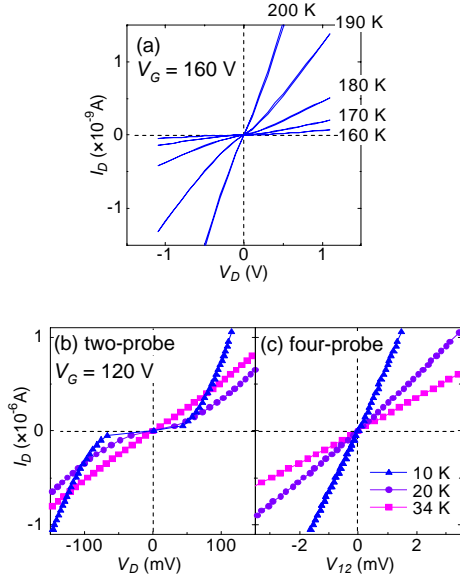


FIG. 2: Current-voltage characteristics of parylene/SrTiO<sub>3</sub>-FETs at low temperatures. (a) Typical drain current–drain voltage ( $I_D$ – $V_D$ ) characteristic for a device with a parylene gate insulator deposited in low vacuum ( $10^{-3}$ – $10^{-2}$  Pa). (b)  $I_D$ – $V_D$  curves for a device with a parylene gate insulator deposited at higher vacuum ( $10^{-4}$  Pa). (c) Same sample as (b) where  $I_D$  is plotted against the voltage difference  $V_{12}$  between the two potential probes inside the channel. The parylene thickness was  $0.53 \mu\text{m}$  for both of devices.

in general require such high vacuum. Finally, gold was evaporated for a gate electrode. All the transport measurements were carried out by Agilent E5287A high-resolution source/monitor unit modules equipped on an E5270B. Variable temperature was obtained by using a Quantum Design physical property measurement system.

As noted above, our SrTiO<sub>3</sub>-FET with a parylene gate insulator deposited in low vacuum has poor carrier injection from the source/drain electrodes at low temperature. Figure 2(a) shows typical drain current–drain voltage ( $I_D$ – $V_D$ ) characteristics of the device prepared at low vacuum, where  $I_D$  goes below the noise level below around 150 K. Figure 2(b) shows  $I_D$ – $V_D$  curves of the device prepared at higher vacuum, indicating the successful carrier injection at low temperatures. Nonlinear  $I_D$ – $V_D$  characteristics are still observed in the small  $V_D$  region. Fig. 2(c) shows those of  $I_D$ – $V_{12}$ , where  $V_{12}$  is the potential drop inside the channel measured by the two potential probes. Ohmic behavior in Fig 2(c) clearly indicate barrier formation at the SrTiO<sub>3</sub>/Al interfaces, which prevents carrier injection and opens a gap in the small  $V_D$  region in Fig 2(b). It is necessary to lower the barrier at the Al/SrTiO<sub>3</sub> interface for efficient carrier injection at low temperatures.

Now we turn to the details of the low-temperature characteristics of the SrTiO<sub>3</sub>-FET. Figure 3 shows the sheet resistance  $R_{\square}$  as a function of the gate voltage  $V_G$  at 8 K. Gate leakage current  $I_G$  is much smaller than  $I_D$ ,

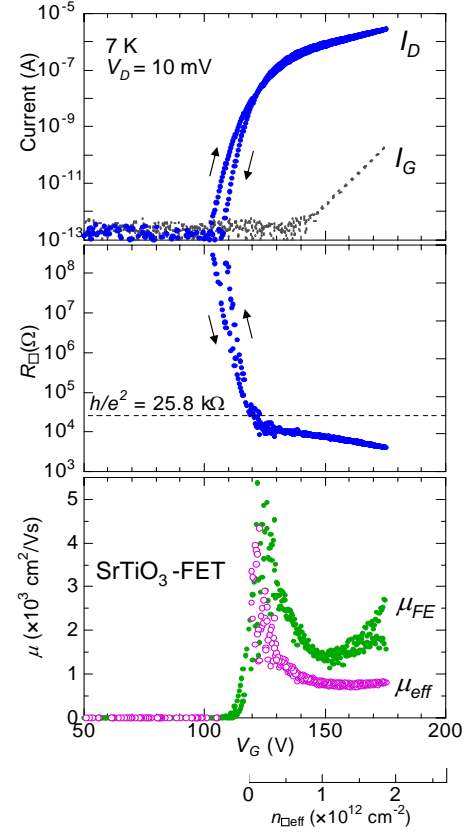


FIG. 3: The drain current,  $I_D$ , the gate leakage current,  $I_G$ , the sheet resistance,  $R_{\square}$ , and the mobility,  $\mu$ , are plotted against the gate voltage,  $V_G$ . The measurement was carried out under constant drain voltage of 10 mV. The arrows indicate the sweep direction of the gate voltage, and the observed hysteresis is probably due to traps at the parylene/SrTiO<sub>3</sub> interface. Sheet resistance was defined as  $R_{\square} = (W/D) \cdot (I_D/V_{12})$ , where  $V_{12}$  is the voltage drop between two potential probes,  $D$  is the distance between the two probes, and  $W$  is the channel width. A scale of the effective (mobile) electron density,  $n_{\square\text{eff}}$ , is also shown at the bottom.

as also plotted in Fig. 3, which assures the accuracy of the measured sheet resistance. As  $V_G$  is increased, the effective sheet carrier density  $n_{\square\text{eff}} = C_i(V_G - V_{G\text{th}})$  is increased. Here,  $V_{G\text{th}}$  is the threshold voltage of  $\sim 118$  V determined from a linear fit of the  $\sqrt{I_D}$ – $V_G$  curve, and  $C_i = 5.3 \text{ nF/cm}^2$  is the capacitance per unit area of the parylene gate insulator. With increasing  $n_{\square\text{eff}}$ ,  $R_{\square}$  decreases drastically from more than G $\Omega$  to the order of k $\Omega$ .

There are two points to be noted in the middle panel of Fig. 3. First,  $R_{\square}$  becomes smaller than the quantum resistance,  $h/e^2 \sim 25.8 \text{ k}\Omega$ . Therefore, the channel region at higher gate voltages can be metallic. A rough estimate of the thickness of the conducting layer in the SrTiO<sub>3</sub>-FET is less than 10 nm [3]. Recent studies on two dimensional electron systems such as Si-MOSFET or p-GaAs showed that a metal-insulator transition occurs when the sheet resistance is the order of the quantum resistance [9]. The

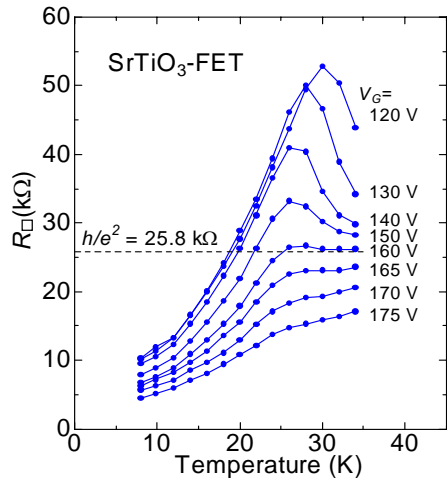


FIG. 4: Sheet resistance  $R_{\square}$  as a function of temperature for gate voltages  $V_G$  of 120–175 V. The parylene gate insulator thickness is 0.53  $\mu\text{m}$ .

second point is the presence of an “inflection point” in the  $R_{\square}-V_G$  curve around 120 V. This point seems to reflect a qualitative change in the electronic state of the channel. Indeed, the value of  $R_{\square}$  at the inflection point is almost identical to the quantum sheet resistance, underpinning the insulator-to-metal transition in this system.

The large threshold  $V_{G\text{th}}$  observed in Fig. 3 may be due to a high density of traps ( $\sim 10^{12} \text{ cm}^{-2}$ ) located at the SrTiO<sub>3</sub> surface. Only when we apply sufficient gate voltage to fill the traps, mobile electrons accumulate. To estimate the mobility of the itinerant carriers, we consider two alternative expressions: field-effect mobility,  $\mu_{\text{FE}}$ , and the effective mobility,  $\mu_{\text{eff}}$ . They are defined as follows:

$$\mu_{\text{FE}} = \frac{\partial}{\partial n_{\square}} \left( \frac{1}{R_{\square}} \right) = \frac{1}{C_i} \frac{\partial}{\partial V_G} \left( \frac{1}{R_{\square}} \right)$$

$$\mu_{\text{eff}} = \frac{1}{qn_{\square\text{eff}}R_{\square}}$$

The difference is that  $\mu_{\text{eff}}$  needs input of the effective

sheet carrier density  $n_{\square\text{eff}}$ , whereas  $\mu_{\text{FE}}$  does not. The calculated mobilities are shown in the bottom panel of Fig. 3. There are no significant difference between the two mobilities. They are as high as 1000–2000  $\text{cm}^2/\text{Vs}$ , which is the highest mobility ever attained in an SrTiO<sub>3</sub>-based FET[6, 7, 10, 11, 12]. The large mobility supports our inference that a metallic state is induced by a large gate electric field at the surface of SrTiO<sub>3</sub> at low temperatures. To further confirm this, the temperature dependence of sheet resistance has been measured. Figure 4 shows  $R_{\square}(T)$  curves taken at eight different gate voltages; the larger gate voltage corresponds to the larger carrier density. Apparently, metallic behavior ( $dR_{\square}/dT > 0$ ) is observed down to 8 K, which is the lowest accessible temperature of the present measurement.

It is interesting to note the presence of the anomaly around 25 K in Fig. 4. This anomaly becomes more prominent with decreasing carrier density until a peak is formed in the  $R_{\square}(T)$  curve. Above the characteristic temperature of the  $R_{\square}(T)$  anomaly (25 K–30 K), the  $R_{\square}(T)$  curves can be classified into two groups: insulating behavior ( $dR_{\square}/dT > 0$ ) and metallic behavior ( $dR_{\square}/dT < 0$ ). Interestingly, at the border between these two behaviors, where the plateau in  $R_{\square}(T)$  curve is observed ( $V_G \sim 160$  V), the sheet resistance is very close to  $h/e^2$ .

In summary, improvement of the fabrication process of single-crystalline SrTiO<sub>3</sub>-based FET, has led to the finding that the surface of the undoped SrTiO<sub>3</sub> turns into a high-mobility ( $>1000 \text{ cm}^2/\text{Vs}$ ) conducting state by applying a large gate electric field at low temperatures. Temperature dependence of the sheet resistance  $R_{\square}$  suggests the high-mobility state is indeed metallic ( $dR_{\square}/dT > 0$ ), with  $R_{\square}$  below the quantum resistance for  $V_G > 160$  V. Field-induced superconductivity of undoped SrTiO<sub>3</sub> is our current target for further deployment of this technique.

This work is partially supported by Grant-in-Aid for Scientific Research from MEXT, Japan. We thank H. Y. Hwang for discussion and critical reading of the manuscript.

- 
- [1] M. Imada, A. Fujimori, and Y. Tokura, Rev. Mod. Phys. **70**, 1039 (1998).
  - [2] C. H. Ahn, J.-M. Triscone, and J. Mannhart, Nature (London) **424**, 1015 (2003).
  - [3] I. H. Inoue, Semicond. Sci. Technol. **20**, S112 (2005).
  - [4] O. N. Tufte and P. W. Chapman, Phys. Rev. **155**, 796 (1967).
  - [5] C. S. Koonce, Marvin L. Cohen, J. F. Schooley, W. R. Hosler, and E. R. Pfeiffer, Phys. Rev. **163**, 380 (1967).
  - [6] K. Ueno, I. H. Inoue, H. Akoh, M. Kawasaki, Y. Tokura, and H. Takagi, Appl. Phys. Lett. **83**, 1755 (2003).
  - [7] K. Shibuya, T. Ohnishi, M. Lippmaa, M. Kawasaki, and H. Koinuma, Appl. Phys. Lett. **85**, 425 (2004).
  - [8] M. Kawasaki, K. Takahashi, T. Maeda, R. Tsuchiya, M. Shinohara, O. Ishiyama, T. Yonezawa, M. Yoshimoto, and H. Koinuma, Science **266**, 1540 (1994).
  - [9] S. V. Kravchenko and M. P. Sarachik, Rep. Prog. Phys. **67**, 1 (2004)
  - [10] I. Pallecchi, G. Grassano, D. Marre, L. Pellegrino, M. Putti, and A. S. Siri, Appl. Phys. Lett. **78**, 2244 (2001).
  - [11] F. Pan, D. Olaya, J. C. Price, and C. T. Rogers, Appl. Phys. Lett. **84**, 1573 (2004).
  - [12] K. S. Takahashi, D. Matthey, D. Jaccard, J.-M. Triscone, K. Shibuya, T. Ohnishi, and M. Lippmaa, Appl. Phys. Lett. **84**, 1722 (2004).